Ab initio molecular dynamics simulations of molten Al_{1−x}Si_{x} alloys

K. H. Khoo, T.-L. Chan, M. Kim, and James R. Chelikowsky

Phys. Rev. B **84**, 214203 — Published 21 December 2011

DOI: 10.1103/PhysRevB.84.214203

Ab-Initio Molecular Dynamics Simulations of Molten $Al_{1-x}Si_x$ Alloys

K. H. Khoo[1], T.-L. Chan[2], M. Kim[3], and James R. Chelikowsky[4]

[1]*Department of Materials Science and Engineering, Institute of High Performance Computing, Singapore 138632, Singapore*

[2]*Department of Physics, The Hong Kong Baptist University, Kowloon Tong, Hong Kong*

[3]*Department of Chemical Engineering, University of Texas, Austin, Texas 78712, USA*

[4]*Center for Computational Materials, Institute for Computational Engineering and Sciences, Departments of Chemistry and Biochemistry, and Physics, University of Texas, Austin, Texas 78712, USA*

Abstract: Recent increases in computational efficiency have enabled large-scale *ab-initio* molecular dynamics simulations to be performed on molten eutectic $Al_{1-x}Si_x$ alloys (x=0.12). Atomic forces were calculated using real-space pseudopotential density-functional theory and the pair correlation, structure factor, coordination number, velocity autocorrelation, and mean-square displacement were computed at temperatures 973K, 1223K, and 1473K. The calculated structure factor agrees very well with data from neutron diffraction experiments. In addition, an analysis of partial coordination numbers suggests that Si and Al are well-mixed. This finding does not support an earlier conjecture attributing anomalous density variations to Si-aggregation phenomena. However, a more definitive conclusion on this hypothesis requires larger simulations over longer time scales. For dynamical properties, the velocity autocorrelation function calculated for Al atoms demonstrates a "cage effect," similar to that found in pure liquid Al. In addition, the diffusion constants of Al are consistently lower than that of Si over the temperature range we have studied.

1. Introduction

There has been active interest in Al–Si binary liquid alloys both from a scientific and applications perspective. Si-doped Al demonstrates increased corrosion resistance and a reduced thermal expansion coefficient, as well as improved machining characteristics relative to Al. All these benefits are achieved while retaining the characteristic high strength-over-weight ratio, enabling its usage in aerospace and automobile industry applications.[1]

From a fundamental scientific perspective, liquid alloys exhibit interesting properties such as anomalies in resistivity, density, and surface tension as well as a Knight shift.[2] It has also been shown experimentally that these liquid alloys have microstructural properties that depend on details of the growth process. Specifically, X-ray diffraction studies have demonstrated that microstructures in Al-13 wt.% Si alloys can be altered by a superheating of the melt followed by a rapid cooling.[3] A discontinuity in the volume expansion coefficient was also observed in density measurements of liquid Al-Si alloys using the sessile drop method.[4] This discontinuity is accompanied by the appearance of a pre-peak in the X-ray diffraction structure factor, and these observations were postulated to arise from a segregation of Si clusters in the superheated melt. Additional evidence of the formation of microstructural inhomogeneities has been provided by a more recent experimental study.[5] On heating eutectic and hypereutectic samples of liquid Al-Si from 973K to 1473K, inhomogeneities with sizes between 10Å to 900 Å were detected using small angle neutron scattering (SANS), and the formation of these "clusters" were only partly reversible upon cooling. However, the authors of this work did not speculate about the origins of these inhomogeneities. There have also been numerous diffraction studies on liquid Al-Si alloys, but structure factors measured at similar compositions and temperatures exhibited measurable differences and spread.[3-7] The search for the origin of the observed microstructures and a lack of consensus on the measured structure factors makes this an interesting system for further study.

There have been several theoretical studies of liquid Al-Si employing *ab-initio* molecular dynamics (AIMD).[7-10] The pair correlation function, structure factor, velocity autocorrelation, mean square-displacement, and diffusion constant were studied as a function of liquid temperature and composition and these studies have given valuable insight into these systems. However, owing to the high computational cost of *ab-initio* calculations, the system sizes studied are relatively small (50-200 atoms). In particular, these system sizes exclude the possibility of studying segregation and clustering phenomena. In addition, there are also non-negligible differences in the calculation results, possibly arising from finite size effects.

Here, MD simulations employing a real-space pseudopotential density functional theory (DFT) formalism was used to study a variety of static and dynamical properties of eutectic liquid Al-Si

alloys over a range of temperatures. Our work extends earlier studies by exploring larger system sizes containing up to 500 atoms and longer simulation times up to 10 ps. This increase in scale is made possible by the development of a Chebyshev-filtering algorithm that significantly speeds-up the solution of the Kohn-Sham equations. More details on this method can be found elsewhere.[11,12] Our aim is to understand the clustering behavior in superheated alloys and to resolve the discrepancy between various measured and calculated structure factors. Another difference between the current and previous work is that we perform microcanonical simulations where the total energy is conserved, while earlier simulations employ an external thermostat to keep the temperature stable.[13] An advantage of performing constant energy simulations is that there are no external perturbations that might affect the calculation results, particularly ones that are sensitive to perturbations such as dynamical properties.

2. Methodology

In our calculations, we employ the real-space pseudopotential DFT formalism and perform Born-Oppenheimer molecular dynamics (BOMD), where a fully self-consistent solution of the Kohn-Sham equation is obtained at every time step.[14, 15] Ion dynamics were generated using Hellman-Feynman forces together with the Beeman algorithm using a time step of 248 a.u. (6 fs).[16] Convergence tests performed using 4 fs and 6 fs time steps yield nearly identical structure factor and velocity autocorrelation functions. An efficient extrapolation of the charge density and wave functions was also implemented to provide a better initial basis for filtering at every time step.[17] Wavefunctions as well as potentials were represented on a uniform real-space grid, giving rise to a sparse Hamiltonian. Recently, we have made a significant algorithmic advance to our density-functional method using the Chebyshev-filtered subspace iteration technique.[11, 12] In this new algorithm, the "standard" diagonalization at each self-consistent field iteration (SCF) is replaced by a Chebyshev subspace filtering step, resulting in a speed up of an order of magnitude or more. (One MD time step on a 500 atom system takes about 30 minutes wall clock time on 64 Cray XT4 processors.) Ion cores were represented by pseudopotentials generated using the reference configurations $[Ne]3s^2 3p^1$ with a cutoff radius of 2.4 au for Al and $[Ne]3s^2 3p^2$ with a cutoff radius of 2.4 au for Si.[18] Cubic supercells were employed for all calculations and the grid spacing was selected to be as close to 0.70 a.u. as possible while maintaining commensurability. The

local-density approximation as parametrized by Ceperley and Alder was used for exchange correlation and the Γ-point was sampled in the Brillouin zone.[19]

Simulations were performed for the eutectic mixture $Al_{0.88}Si_{0.12}$ in 200 atom and 500 atom supercells at target temperatures 973K, 1223K, and 1473K. These temperatures were chosen to correspond to those in recent SANS measurements of liquid Al-Si alloys[5] and supercell sizes were chosen to give number densities corresponding to $n_{973K} = 0.0519$ Å^{-3}, $n_{1223K} = 0.0504$ Å^{-3}, and $n_{1473K} = 0.0489$ Å^{-3}, values derived from sessile drop measurements.[4] To set up the calculation, atoms were placed at random inside the cubic supercell while taking care to prevent any two atoms from getting too close to each other. The system was then coupled to a virtual heat bath via Langevin equations of motion,[20] at a temperature far above the target value, and propagated in time to eradicate any memory of its initial configuration. The system was then cooled down gradually at a rate of 0.417 K/fs to the target temperature and decoupled from the heat bath where a microcanonical simulation was carried out for 10.0 ps and 4.0 ps for the 200 atom and 500 atom systems respectively. The data collected from the microcanonical part of our simulations were then used for computing the properties of liquid Al-Si alloys. Energy conservation constitutes a stringent test of the accuracy for ionic forces, as any systematic error in the forces will prevent conservation of total energy. The total energy drift for our simulations was found to be consistently less than 1 meV/ps or nearly negligible.

3. Results and Discussion

The pair correlation function $g(r)$ is often used to characterize structural properties of noncrystalline solids and liquids. It is defined as the probability of finding a pair of atoms a distance r apart relative to the probability expected for a completely random distribution at the same density. However, in diffractions experiments, different elements will contribute differently to the total intensity. Thus one needs to calculate an averaged total $g(r)$ from the partial pair correlation functions $g_{ij}(r)$, appropriately weighted with the atomic scattering lengths for X-ray scattering or atomic form factors for neutron scattering. Following the Faber-Ziman formalism,[21] the total pair correlation $g(r)$ is given in terms of the partial pair correlation functions $g_{ij}(r)$ by

$$g(r) = \frac{1}{\langle b \rangle^2}\left(x_i^2 b_i^2 g_{ii}(r) + 2x_i x_j b_i b_j g_{ij}(r) + x_j^2 b_j^2 g_{jj}(r)\right) \quad \text{where } \langle b \rangle = x_i b_i + x_j b_j \tag{1}$$

Here, i, j are atom types, x_i, x_j are the molar fractions, and b_i, b_j are atomic scattering lengths or atomic form factors for X-ray and neutron scattering respectively. The ratio of the neutron scattering lengths are b_{Al}/b_{Si} = 0.8313 and that of X-ray form factors are b_{Al}/b_{Si} = 0.9286 under typical experimental conditions.[22, 23]

In Fig. 1a, we plot the functions $G(r) = r(g(r) - 1)$ and $G_{ij}(r) = r\left(g_{ij}(r) - 1\right)$ of liquid $Al_{0.88}Si_{0.12}$, where $g_{ij}(r)$ and $g(r)$ are the partial and total pair correlation functions respectively. Here, $g(r)$ is computed using the neutron scattering lengths listed above. The first peak of $G(r)$ decreases in height with increasing temperature and the peak position is nearly fixed at ~2.80 Å, showing only modest increases with temperature. The amplitude changes reflect a decrease in the ordering of the liquid while the peak positions are mainly affected by composition. Similar but less pronounced changes also happen at the second peak, with decreasing peak heights and constant peak positions as the temperature is increased. These trends are also replicated for the first peaks of $G_{Al\text{-}Al}(r)$ and $G_{Al\text{-}Si}(r)$, as can be seen in the figure. Another observation we could make is that the first peak positions of $G_{Al\text{-}Al}$ (2.77 Å) and $G_{Si\text{-}Si}$ (2.46 Å) are fairly similar to those in pure liquid Al (2.74 Å) and liquid Si (2.43 Å).[12,15] This suggests that the Al-Al and Si-Si interactions in liquid Al-Si alloys are not too different from those of pure liquids.

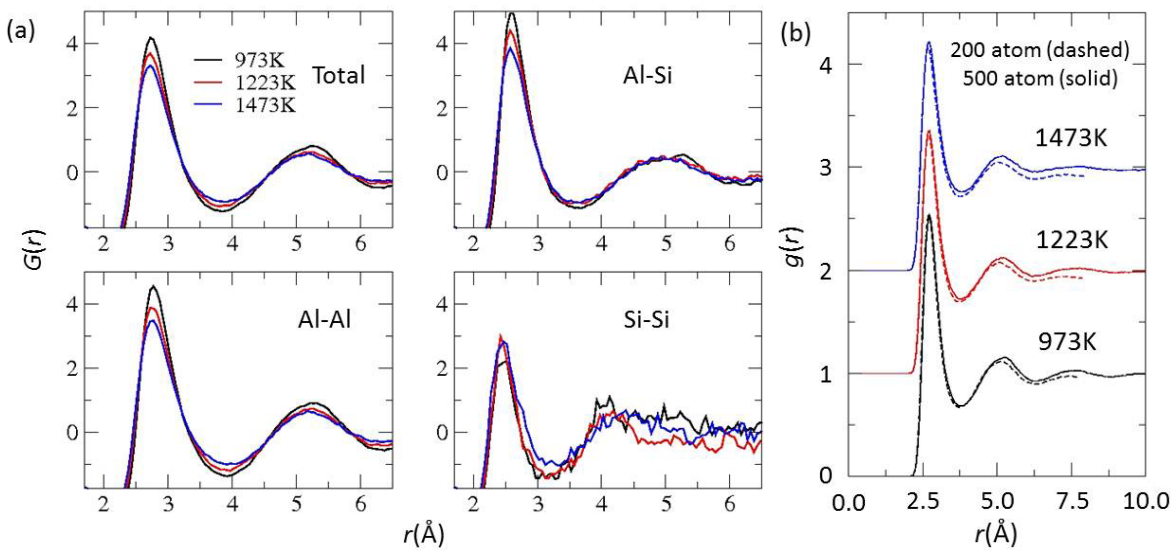

Fig 1: (a) $G(r) = r(g(r) - 1)$ derived from the partial and total pair correlation functions for liquid $Al_{0.88}Si_{0.12}$ calculated at 973K, 1223K and 1473K from 500 atom simulations. (b) Comparison of the total pair correlation function calculated from 200 atom (dashed lines) and 500 atom (solid lines) simulations for several target temperatures.

Unlike the other partial pair correlation functions, the statistics for $G_{Si\text{-}Si}$ are still insufficient to give a smooth plot, owing to the low proportion of Si atoms in the system. Despite the noise, one can still establish a clear increasing trend of the first peak amplitude with increasing temperature. This is consistent with previous theoretical work and indicates an increasing tendency of Si atoms to aggregate at higher temperatures in liquid Al-Si.[8] However, the amplitude of the first peak in $G_{Al\text{-}Si}$ is still larger than that of $G_{Al\text{-}Al}$ and $G_{Si\text{-}Si}$ for all our simulated temperatures, implying that Al and Si nearest neighbors pairings are preferred relative to Si-Si or Al-Al ones. In Fig. 1b, a measure of convergence in our results is obtained by plotting $g(r)$ from 200 atom and 500 atom simulations. The curves from the smaller and larger simulations are quite similar and fairly well converged, showing only slight deviation at larger r values.

From the partial pair correlation functions, we can obtain the partial structure factors by performing a Fourier transform according to the following relation

$$S_{ij}(k) = 1 + 4\pi\rho \int \left(g_{ij}(r) - 1\right) \frac{sin(kr)}{k} r\, dr \qquad (2)$$

These partial structure factors can then be combined using the Faber-Ziman formalism to yield the total structure factor $S(k)$

$$S(k) = \frac{1}{\langle b \rangle^2} \left(x_i^2 b_i^2 S_{ii}(k) + 2x_i x_j b_i b_j S_{ij}(k) + x_j^2 b_j^2 S_{jj}(k) \right) \qquad (3)$$

where x_i, b_i , and $\langle b \rangle$ have similar meanings as in eqn. 1. Structure factors are very useful quantities to know as they can be measured directly from neutron or X-ray scattering. $S(k)$ simulated using 500 atom supercells and calculated employing neutron scattering lengths for b_i are plotted in Fig. 2a for various target temperatures. The simulated structure factor has its first peak at ~2.71 $Å^{-1}$ and the position of this peak is nearly independent of temperature, behavior reminiscent of $g(r)$. Also, the peak height decreases as the temperature is increased, indicative of increasing disorder. In Fig. 2b, our 973K result is plotted together with neutron diffraction data collected at the same temperature.[5] The experimental and calculated $S(k)$ show very good agreement, with the only deviation being a slight discrepancy in the height of the 1st peak. Such findings give us confidence in the accuracy of our results.

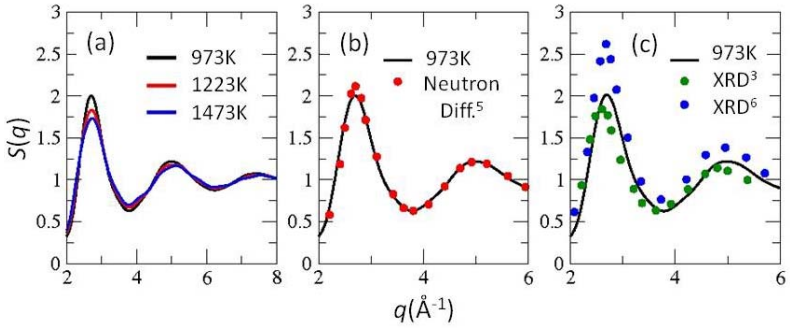

Fig 2: (a) Simulated total structure factor for $Al_{0.88}Si_{0.12}$ at 973K, 1223K and 1473K. (b) Structure factor at 973K from simulations and neutron diffraction data (Ref. 5). (c) Simulated structure factor at 973K and results from X-ray diffraction at 948K (Refs. 3 and 6).

For comparison with X-ray diffraction experiments, we re-computed the total structure factor using X-ray atomic form factors for b_i in eqn. 3. The resulting $S(k)$ for $T = 973$K is plotted in Fig. 2c, along with data collected from two separate XRD experiments at 948K.[3,6] We expect the small temperature mismatch between experiment and theory to have a relatively small effect on the structure factor. We also find that our $S(k)$ generated for neutron and X-ray scattering to be very similar, with both curves having the same peak positions and peak heights differing by less than 1%. In Fig. 2c, we see non-negligible differences between our results and the experimental XRD spectra, as well as between the two XRD measurements themselves. It has been suggested that inaccuracies in the experiments may be the source of these disagreements,[5] as the results in Refs. 3 and 6 show a very large spread. Our findings are consistent with this claim.

Next, let us investigate the extent of mixing and segregation between Al and Si atoms by calculating coordination numbers using the following expression.

$$N_{ij} = \rho x_j \int_0^{R_{min}} 4\pi r^2 g_{ij}(r) dr \qquad (4)$$

Here, R_{min} is the position of the 1st minima in the $g_{ij}(r)$ curve, N_{ij} the average number of jth-type atoms in the first atomic shell of an ith-type atom, and x_i the mole fraction of ith-type atoms. R_{min} for g, $g_{Al\text{-}Al}$, $g_{Al\text{-}Si}$, and $g_{Si\text{-}Si}$ are ~ 3.8Å, 3.9 Å, 3.5 Å, and 3.1 Å respectively and the results are listed in table 1.

	$T = 973$K	$T = 1223$K	$T = 1473$K
N_{tot}	11.4	11.0	10.6
$N_{Al\text{-}Al}$	10.7	9.8	9.4
$N_{Al\text{-}Si}$	1.2	1.1	1.0
$N_{Si\text{-}Al}$	8.7	7.8	7.5
$N_{Si\text{-}Si}$	0.50	0.57	0.63

Table 1: Partial and total coordination numbers of liquid $Al_{0.88}Si_{0.12}$ alloy at temperatures 973K, 1223K and 1473K.

From the Table, we see that N_{tot} decreases with increasing temperature, indicative of a tendency for the liquid to adopt a more open structure at higher temperatures. The same temperature dependence applies for $N_{Al\text{-}Al}$, $N_{Al\text{-}Si}$, and $N_{Si\text{-}Al}$, with only $N_{Si\text{-}Si}$ increasing with increasing temperatures. The trends for these partial coordination numbers are similar to that of the first peak in g_{ij}. Also, the coordination number for Al at 973K (~11.38) is very similar to that of pure liquid Al at 1000K (~11.4). This is reasonable considering the closeness of the simulation temperatures and the large mole fraction of Al in this simulation.[15] To get more information about the coordination of atoms in these binary liquids, we plot the distribution of the number of nearest neighbor atoms about Al and Si atoms in Fig. 3a for T = 973K. The most prevalent coordination for Al is 12, with the distribution centered around 9 to 15 nearest neighbors. For Si, the distribution is pretty similar to that of Al but shifted to the left, with the most common coordination being 9 and the distribution spread around 6 to 12 nearest neighbors.

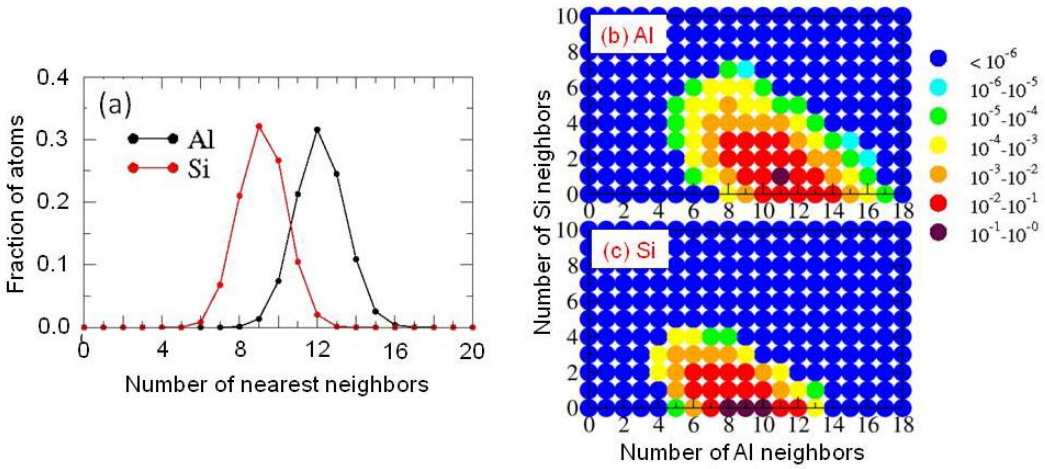

Fig. 3: (a) Distribution of Al (black) and Si (red) atoms by number of nearest neighbor atoms. (b) Fraction of Al atoms having specific Al and Si coordination numbers. (c) Same as in (b) but for Si atoms.

To investigate the aggregation of atoms of similar chemical species, we can plot the distribution of atoms having specific numbers of Al and Si nearest neighbors, and this is shown in Figs. 3b and 3c. The most prevalent coordination for Al contains 11 Al and 1 Si atom in the nearest neighbor shell, as seen in Fig. 3b. The ratio of Al to Si nearest neighbors is close to that expected

of a random distribution, suggesting that the system is well-mixed chemically. In addition, we see that a total coordination of 12 nearest neighbors is favored for all Al-to-Si nearest neighbor ratios, consistent with the results in Fig. 3a. In Fig. 3c, we plot the corresponding distribution for Si atoms. The shape of the distribution is very similar to that of Al, with the most common coordination being a Si atom surrounded by 9 Al and no Si atoms. There are in fact very few Si atoms having more than 2 Si nearest neighbors and virtually none having more than 4. Thus our study is unable to provide any evidence of Si aggregation, postulated to explain anomalous density variations and SANS features observed in experiment.[4,5] However, our result does not preclude the possibility of Si aggregation either, particularly considering that clustering phenomena typically occurs over length and time scales larger than ones considered in our simulation. It can also be seen from this plot that a total coordination of 9 about Si is preferred for all Al-to-Si nearest neighbor ratios, consistent with the results of Fig. 3a.

Next, we investigate some single-particle dynamical properties. For these properties, we use data from the smaller 200 atom supercell simulations, but over a longer simulation time of 10 ps, as dynamical properties take longer to converge. First, we look at the velocity autocorrelation functions defined by

$$Z_\alpha(t) = \frac{\langle \sum_{i\in\alpha} \boldsymbol{v}_i(0).\boldsymbol{v}_i(t) \rangle}{\langle \sum_{i\in\alpha} \boldsymbol{v}_i(0).\boldsymbol{v}_i(0) \rangle} \quad (5)$$

where $\boldsymbol{v}_i$ refers to the velocity of the ith atom, α is the chemical species label, and the angular brackets < > referring to an ensemble average. Here, we plotted $Z(t)$ for both Al and Si atoms at 973K, 1223K, and 1473K in Figs. 4a and 4b respectively.

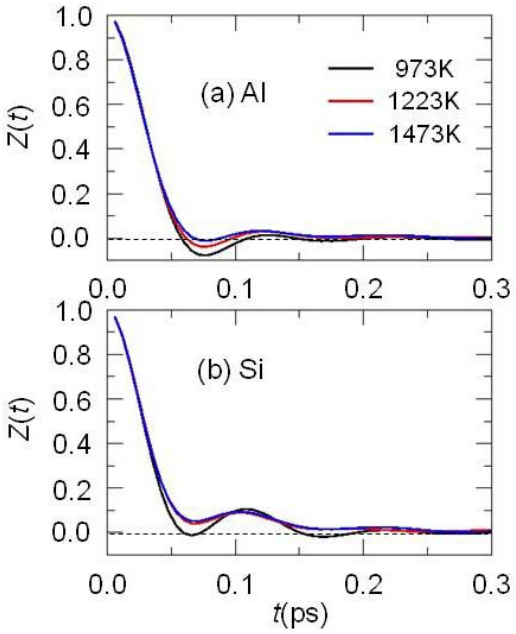

Fig 4: (a) Velocity autocorrelation function for Al atoms at 973K, 1223K and 1473K. (b) Velocity autocorrelation for Si atoms at the same temperatures.

The plots of $Z(t)$ for Al in Fig. 4a can be compared to earlier simulation results for pure liquid Al at T = 1000K.[12] Our current result for 973K shows very similar qualitative behavior to that of pure Al owing to the closeness of the simulation temperatures and the large fraction of Al atoms present in our liquid alloy. In particular, there is a "cage effect" present in both the liquid alloy and pure Al, where atoms surrounding an Al atom allow the latter to move over short distances but then reflect it, causing $Z(t)$ to change sign.[24] This feature is very characteristic of simple metals close to their melting point. Also, as the temperature is increased, there is an overall increase in $Z(t)$ and features in the curve (such as peaks and troughs) become less pronounced. In particular, we notice that the "cage effect" is diminished at higher temperatures and nearly disappears at T = 1473K. For Si, $Z(t)$ is consistently higher than that of Al at the same temperature, and it shows the same trends for increasing temperatures, namely increased $Z(t)$ and less pronounced features. Another quantity that can be extracted from the velocity autocorrelation is the diffusion constant, using the following relation

$$D = \frac{k_B T}{M} \int_0^\infty Z(t)dt \tag{6}$$

where M is the atomic mass and k_B the Boltzmann constant. From this formula, we get diffusion constants for Al as D_{Al} = 0.84 Å^2/ps, 1.27 Å^2/ps, and 1.56 Å^2/ps and that of Si as D_{Si} = 0.96 Å^2/ps, 1.42 Å^2/ps, and 1.75 Å^2/ps for temperatures T = 973K, 1223K, and 1473K respectively. It can be seen that D_{Si} is consistently larger than D_{Al} for all temperatures. Also, as one would expect, the diffusion constants all increase with increasing temperature.

Another dynamical quantity that can be easily computed from our data is the mean-squared displacement of atoms. Elementary considerations show that this quantity should vary linearly in time and is related to the diffusion constant by the following equation.[25]

$$\Delta R_\alpha(t)^2 = \langle \frac{1}{N_\alpha} \sum_{i\in\alpha} |\boldsymbol{r}_i(t) - \boldsymbol{r}_i(0)|^2 \rangle = 6D_\alpha t + c \tag{7}$$

where α is the chemical species, r_i are coordinates of the ith atom, N_α is the number of atoms of chemical species α in the simulation cell, and c is a constant. These quantities are plotted in Fig. 5a and 5b for Al and Si atoms respectively. The linear behavior can be clearly seen and the gradient increases with temperature, as expected from Eq. 7.

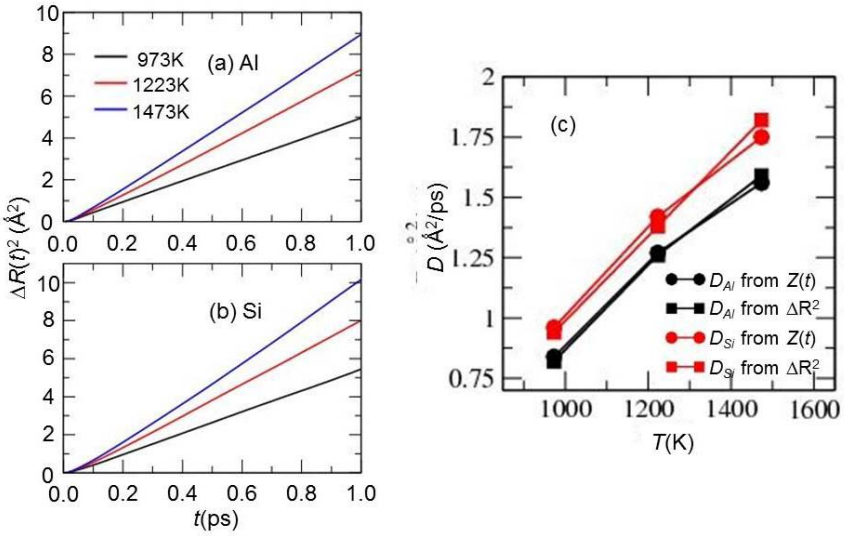

Fig 5: Mean squared displacement for (a) Al and (b) Si atoms as function of time. (c) Diffusion constants as function of temperature obtained from eqns. 6 and 7.

In Fig. 5c, we plot the diffusion constants D_{Al} and D_{Si} estimated from both $Z(t)$ and ΔR^2. There is very good agreement between these estimates. This is an indication of the quality of our simulation. In particular, our results are derived from a microcanonical simulation where N, V, and E are constant. These tend to generate higher quality results than simulations utilizing a thermostat to reach a target temperature, as the thermostat is constantly perturbing the system and altering measured properties.

Conclusions

In this work, we have performed AIMD simulations on liquid $Al_{0.88}Si_{0.12}$ alloys to investigate a variety of static and dynamic properties $g(r)$, $S(k)$, N_{ij}, $Z(t)$, D, and ΔR^2 as a function of temperature. We have compared our calculated structure factors to experimental neutron scattering results and obtained very good agreement. In addition, we have computed the partial and total coordination numbers around Al and Si atoms. We find from this analysis that the liquid is well-mixed and fairly homogeneous. In particular, we find no evidence of Si aggregation in our simulations as postulated in earlier experimental work.[4] However, simulations over larger length and time scales are required to adequately address the validity of this postulate. For dynamical properties, we have found that the velocity autocorrelation of Al atoms in the liquid alloy demonstrates the "cage effect," similar to pure liquid Al. Also, the diffusion constants of Al atoms are consistently lower than that of Si over the temperatures we have studied.

Acknowledgements

This work is supported by the National Science Foundation under Grant No. DMR 09-41645 and the Welch Foundation under Grant No. F-1708. Calculations were performed at the Texas Advanced Computing Center (TACC) from a Teragrid grant No. TG-DMR-090026.

References

[1] H. Ye, J. Mater. Eng. Perform. **12**, 288 (2003).

[2] J. Seerveld, S. Van Till, A. Nguyen, C. Timmer, and J.B. Van Zytveld, J. Phys. F: Met. Phys. **15,** L141 (1985).

[3] X. F. Bian and W. M. Wang, Mat. Lett. **44**, 54 (2000).

[4] W. M. Wang, X. F. Bian, H. R. Wang, Z. Wang, L. Zhang, Z. G. Liu, and J.-M. Lui, J. Mater. Res. **16**, 3592 (2001).

[5] U. Dahlborg, M. Besser, M. Calvo-Dahlborg, G. Cuello, C. D. Dewhurst, M. J. Kramer, J. R. Morris, and D. J. Sordelet, J. Non-Cryst. Solids **353**, 3005 (2007).

[6] X. F. Bian, W. M. Wang, and J. Qin, Mat. Charact. **46**, 25 (2001).

[7] W. M. Wang, X. F. Bian, J. Qin, and G. F. Ton, J. Mater. Sci. Lett. **19**, 1583 (2000).

[8] S. Y. Wang, C. Z. Wang, F.-C. Chuang, J. R. Morris, and K. M. Ho, J. Chem. Phys. **122**, 034508 (2005).

[9] S. Y. Wang, C. Z. Wang, C. X. Zheng, and K. M. Ho, J. Non-Cryst. Solids **355**, 340 (2009).

[10] M. Ji and X. G. Gong, J. Phys.: Condens. Matter **16**, 2507 (2004).

[11] Y. Zhou, Y. Saad, M. L. Tiago, and J. R. Chelikowsky, Phys. Rev. E **74**, 066704 (2006); J. R. Chelikowsky, N. Troullier, and Y. Saad, Phys. Rev. Lett. **72**, 1240 (1994).

[12] K. H. Khoo, M. Kim, G. Schofield, and James R. Chelikowsky, Phys. Rev. B **82**, 064201 (2010).

[13] S. Nose, J. Chem. Phys. **81**, 511 (1984).

[14] J. R. Chelikowsky, J. J. Derby, V.V. Godlevsky, M. Jain, and J. V. Raty, J. Phys.: Condens. Matter **13**, R817 (2001).

[15] M. M. G. Alemany, M. Jain, L. Kronik, and J. R. Chelikowsky, Phys. Rev. B **69**, 075101 (2004).

[16] D. Beeman, J. Comput. Phys. **20**, 130 (1976).

[17] D. Alfe, Comput. Phys. Commun. **118**, 31 (1999).

[18] N. Troullier and J. L. Martins, Phys. Rev. B **43**, 1993 (1991).

[19] D. M. Ceperley and B. J. Alder, Phys. Rev. Lett. **45**, 566 (1980).

[20] N. Binggeli, J. L. Martins, and J. R. Chelikowsky, Phys. Rev. Lett. **68**, 2956 (1992).

[21] T. E. Faber and J. M. Ziman, Phil. Mag. **11**, 153 (1965).

[22] National Nuclear Data Center at Brookhaven National Lab, Neutron News **3**, 29 (1992).

[23] C. T. Chantler, J. Phys. Chem. Ref. Data **29**, 597 (2000).

[24] U. Balucani and M. Zoppi, *Dynamics of the Liquid State* (Clarendon, Oxford, 1994).

[25] J. P. Hansen and I. R. McDonald, *Theory of Simple Liquids* (Academic, London, 1986).